Devil's Staircase Continuum in the Chiral Clock Spin Glass with Competing Ferromagnetic-Antiferromagnetic and Left-Right Chiral Interactions

Tolga Çağlar[1] and A. Nihat Berker[1,2]

[1] *Faculty of Engineering and Natural Sciences, Sabancı University, Tuzla, Istanbul 34956, Turkey*
[2] *Department of Physics, Massachusetts Institute of Technology, Cambridge, Massachusetts 02139, USA*

The chiral clock spin-glass model with $q = 5$ states, with both competing ferromagnetic-antiferromagnetic and left-right chiral frustrations, is studied in $d = 3$ spatial dimensions by renormalization-group theory. The global phase diagram is calculated in temperature, antiferromagnetic bond concentration p, random chirality strength, and right-chirality concentration c. The system has a ferromagnetic phase, a multitude of different chiral phases, a chiral spin-glass phase, and a critical (algebraically) ordered phase. The ferromagnetic and chiral phases accumulate at the disordered phase boundary and form a spectrum of devil's staircases, where different ordered phases characteristically intercede at all scales of phase-diagram space. Shallow and deep reentrances of the disordered phase, bordered by fragments of regular and temperature-inverted devil's staircases, are seen. The extremely rich phase diagrams are presented as continuously and qualitatively changing videos.

PACS numbers: 75.10.Nr, 05.10.Cc, 64.60.De, 75.50.Lk

I. INTRODUCTION

The presence of chiral interactions, motivated by experimental systems [1–5], can result in extremely rich phase transition phenomena in otherwise simple systems [6]. In this respect, we study here a $q = 5$ state clock spin-glass model in $d = 3$ spatial dimensions, using renormalization-group theory. Our system has both competing ferromagnetic and antiferromagnetic interactions, as in the usually studied spin-glass models [7], and competing left-chiral and right-chiral interactions [6].

The global phase diagram is calculated in temperature, antiferromagnetic bond concentration p, random chirality strength, and right-chirality concentration c. We find an extremely rich phase diagram, with a ferromagnetic phase, a multitude of different chiral phases, a chiral spin-glass phase, and a critical (algebraically) ordered phase [8, 9]. The ferromagnetic and chiral phases accumulate at the disordered phase boundary and form a devil's staircases [10, 11], where different ordered phases characteristically intercede at all scales of phase-diagram space. In fact, a continuum of devil's staircases is found. Shallow and deep reentrances of the disordered phase, bordered by fragments of regular and temperature-inverted devil's staircases, are seen. The extremely rich phase diagrams are presented as continuously and qualitatively changing videos.

II. THE $q-$STATE CHIRAL CLOCK DOUBLE SPIN GLASS

The $q-$**state clock spin glass** is composed of unit spins that are confined to a plane and that can only point along q angularly equidistant directions, with Hamiltonian

$$-\beta\mathcal{H} = \sum_{\langle ij\rangle} J_{ij}\vec{s}_i.\vec{s}_j = \sum_{\langle ij\rangle} J_{ij}\cos\theta_{ij}, \qquad (1)$$

where $\beta = 1/k_BT$, $\theta_{ij} = \theta_i - \theta_j$, at each site i the spin angle θ_i takes on the values $(2\pi/q)\sigma_i$ with $\sigma_i = 0, 1, 2, \ldots, (q-1)$, and $\langle ij\rangle$ denotes that the sum runs over all nearest-neighbor pairs of sites. As a ferromagnetic-antiferromagnetic spin-glass system [7], the bond strengths J_{ij}, with quenched (frozen) ferromagnetic-antiferromagnetic randomness, are $+J > 0$ (ferromagnetic) with probability $1-p$ and $-J$ (antiferromagnetic) with probability p, with $0 \le p \le 1$. Thus, the ferromagnetic and antiferromagnetic interactions locally compete in frustration centers. Recent studies on ferromagnetic-antiferromagnetic clock spin glasses are in Refs. [12–14].

In the $q-$**state chiral clock double spin glass** introduced here, frustration also occurs via randomly frozen left or right chirality [6]. The Hamiltonian in Eq. (1) is generalized to random local chirality,

$$-\beta\mathcal{H} = \sum_{\langle ij\rangle}[J_{ij}\cos\theta_{ij} + \Delta\,\delta(\theta_{ij} + \eta_{ij}\frac{2\pi}{q})], \qquad (2)$$

where, for each pair of nearest-neighbor sites $\langle ij\rangle$ with j ahead of i in the coordinate direction, frozen (quenched) $\eta_{ij} = 1$ (left chirality) or -1 (right chirality), and the delta function $\delta(x) = 1\,(0)$ for $x = 0\,(x \ne 0)$. The overall concentrations of left and right chirality are respectively $1-c$ and c, with $0 \le c \le 1$. The strength of the random chiral interaction is Δ/J, with temperature divided out. With no loss of generality, we take $\Delta \ge 0$. Thus, the system is chiral for $\Delta > 0$, chiral-symmetric for $c = 0.5$, chiral-symmetry-broken for $c \ne 0.5$. The global phase diagram is in terms of temperature J^{-1}, antiferromagnetic bond concentration p, random chirality strength Δ/J, and chiral symmetry-breaking concentration c.

III. RENORMALIZATION-GROUP TRANSFORMATION: MIGDAL-KADANOFF APPROXIMATION AND EXACT HIERARCHICAL LATTICE SOLUTION

We solve the chiral clock double spin-glass model with $q = 5$ states by renormalization-group theory, in $d = 3$ spatial dimensions, with length rescaling factor $b = 3$. Our solution is, simultaneously, the Migdal-Kadanoff approximation [15, 16] for the cubic lattice and the exact solution [17–21] for the $d = 3$ hierarchical lattice based on the leftmost graph of Fig. 1. Exact calculations on hierarchical lattices are also currently widely used on a variety of statistical mechanics problems.[22–52].

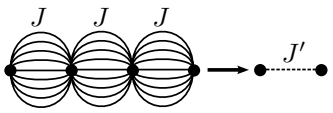

FIG. 1. Renormalization-group transformation consisting of bond moving followed by decimation. The resulting recursion relations are approximate for the cubic lattice, with length-rescaling factor of $b = 3$. The corresponding hierarchical lattice is obtained by the repeated self-imbedding of the leftmost graph. The recursion relations are exact for this $d = 3$ hierarchical lattice.

Under the renormalization-group transformation described below, the Hamiltonian of Eq. (2) maps onto the more general form

$$-\beta\mathcal{H} = \sum_{\langle ij\rangle} V_{ij}(\theta_{ij}), \tag{3}$$

where $\theta_{ij} = \theta_i - \theta_j$ can take q different values, so that for each pair $< ij >$ of nearest-neighbor sites, there are q different interaction constants

$$\{V_{ij}(\theta_{ij})\} = \{V_{ij}(0), V_{ij}(\delta), V_{ij}(2\delta), V_{ij}(3\delta), V_{ij}(4\delta)\} \equiv \mathbf{V}_{ij}, \tag{4}$$

which are in general different at each locality (quenched randomness). Here, $\delta \equiv 2\pi/5$ is the angle between consecutive clock-spin directions. The largest element of $\{V_{ij}(\theta_{ij})\}$ at each locality $< ij >$ is set to zero, by subtracting the same constant G from all q interaction constants, with no effect on the physics; thus, the $q-1$ other interaction constants are negative.

The local renormalization-group transformation is achieved by the sequence, shown in Fig. 1, of bond movings

$$\widetilde{V}_{ij}(\theta_{ij}) - \widetilde{G} = \sum_{k=1}^{b^{d-1}} V_{ij}^{(k)}(\theta_{ij}), \tag{5}$$

and decimations

$$e^{V'_{14}(\theta_{14})-G} = \sum_{\theta_2,\theta_3} e^{\widetilde{V}_{12}(\theta_{12})+\widetilde{V}_{23}(\theta_{23})+\widetilde{V}_{34}(\theta_{34})}, \tag{6}$$

where $\widetilde{G}$ and G are the subtractive constants mentioned above, and prime marks the interaction of the renormalized system.

The starting double-bimodal quenched probability distribution of the interactions, characterized by p and c as described above, is not conserved under rescaling. The renormalized quenched probability distribution of the interactions is obtained by the convolution [53]

$$P'(\mathbf{V}_{i'j'}) = \int \left\{ \prod_{ij}^{i'j'} d\mathbf{V}_{ij} P(\mathbf{V}_{ij}) \right\} \delta(\mathbf{V}_{i'j'} - \mathbf{R}(\{\mathbf{V}_{ij}\})), \tag{7}$$

where $\mathbf{V}_{ij} \equiv \{V_{ij}(\theta_{ij})\}$ as in Eq. (4) and $\mathbf{R}(\{\mathbf{V}_{ij}\})$ represents the bond moving and bond decimation given in Eqs. (5) and (6). Similar previous studies, on other spin-glass systems, are in Refs. [12, 13, 54–65]. For numerical practicality the bond moving and decimation of Eqs. (5) and (6) are achieved by a sequential pairwise combination of interactions, each pairwise combination leading to an intermediate probability distribution resulting from a pairwise convolution as in Eq. (7). We effect this procedure numerically, by generating 1000 interactions that embody the quenched probability distribution resulting from each pairwise combination. Each of the generated 1000 interactions is described by q interaction constants, as explained above (Eq. (4)). At each pairwise convolution as in Eq. (7), 1000 randomly chosen pairs are matched by (5) or (6), and a new set of 1000 interactions is produced.

The different thermodynamic phases of the system are identified by the different asymptotic renormalization-group flows of the quenched probability distribution $P(\mathbf{V}_{ij})$. For all renormalization-group flows, originating inside the phases and on the phase boundaries, Eq. (7) is iterated until asymptotic behavior is reached. Thus, we are able to calculate the global phase diagram of the chiral clock double spin-glass model.

IV. GOBAL PHASE DIAGRAM OF THE $q = 5$ STATE CHIRAL CLOCK DOUBLE SPIN GLASS

The global phase diagram of the $q = 5$ state chiral clock double spin-glass model in $d = 3$ spatial dimensions, in temperature J^{-1}, antiferromagnetic bond concentration p, random chirality strength Δ/J, and right-chirality concentration c, is a four-dimensional object, so that only the cross-sections of the global phase diagram are exhibited.

Figs. 2 show the calculated sequence of phase diagrams for the ferromagnetic ($p = 0$), on the left side of the figure, and antiferromagnetic ($p = 1$), on the right side, systems with quenched random left- and right-chiral interactions. The horizontal axis c is the concentration of right-chiral interactions. Phase diagrams for different random chirality strengths Δ/J are shown. The system exhibits ferromagnetic (F), a multitude of different chi-

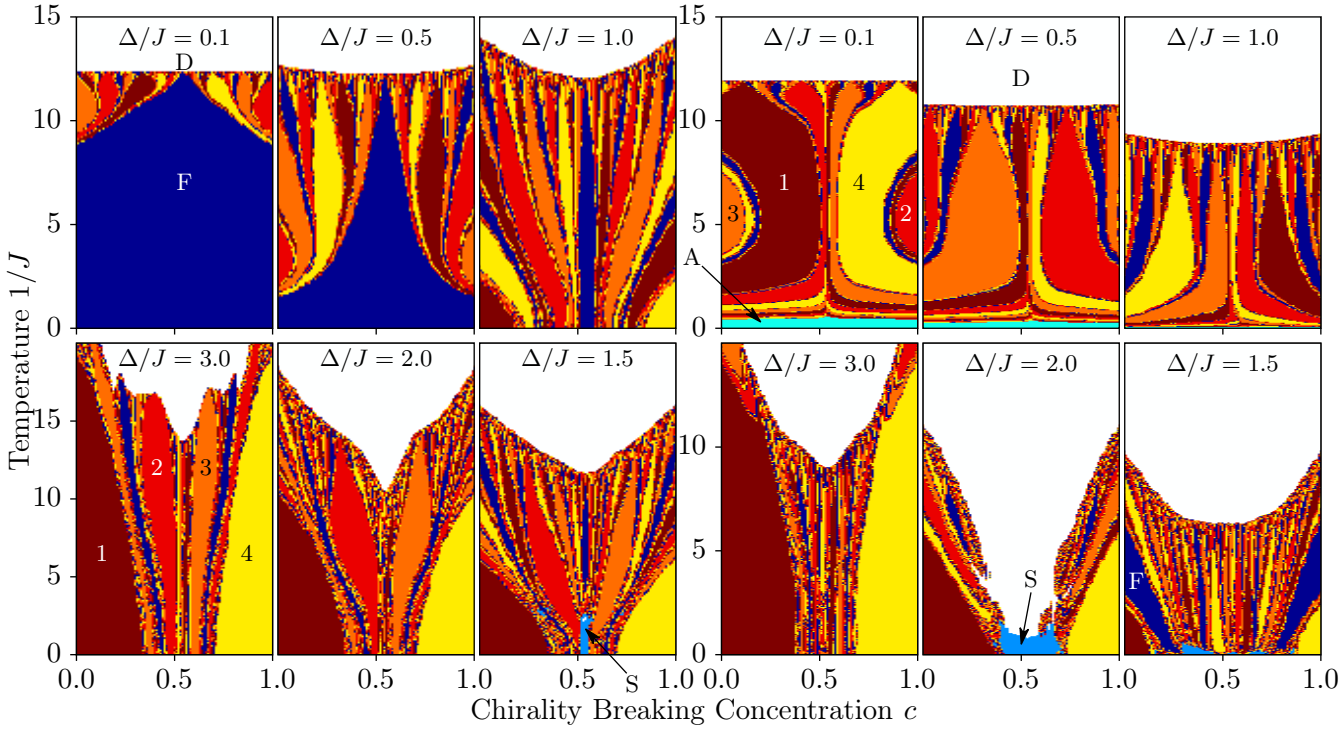

FIG. 2. (Color online) Calculated sequence of phase diagrams for the ferromagnetic ($p = 0$), on the left side of the figure, and antiferromagnetic ($p = 1$), on the right side, systems with quenched random left- and right-chiral interactions. The horizontal axis c is the concentration of right-chiral interactions. Phase diagrams for different random chirality strengths Δ/J are shown. The system exhibits ferromagnetic (F), a multitude of different chiral, and spin-glass (S) ordered phases. On some of the chiral phases, the δ multiplicity of the asymptotically dominant interaction is indicated. The ferromagnetic and chiral phases accumulate as different devil's staircases at their boundary with the disordered (D) phase. The antiferromagnetic system also exhibits an algebraically ordered (A) phase. The full richness of the continuum of widely varying devil's staircase phase diagrams can also be seen in video form, four of which are accessible at http:// web.mit.edu/physics/berker/temperature_Delta_c0_scanp.avi, web.mit.edu/physics/berker/temperature_Delta_c05_scanp.avi, web.mit.edu/physics/berker/temperature_c_p1_scanDelta.avi, web.mit.edu/physics/berker/temperature_c_p0_scanDelta.avi

ral, and spin-glass (S) ordered phases. The antiferromagnetic system also shows an algebraically (A) ordered (critical) phase, in which every point is a critical point with divergent correlation length [8, 9]. In all cases, the ferromagnetic and different chiral phases accumulate as different devil's staircases [10, 11] at their boundary with the disordered (D) phase.

Figs. 3 show the calculated sequence of phase diagrams for the left-chiral ($c = 0$), on the upper side, and quenched random left- and right-chiral ($c = 0.5$), on the lower side, system with in both cases quenched random ferromagnetic and antiferromagnetic interactions. The horizontal axis is the random chirality strength Δ/J. The consecutive phase diagrams are for different concentrations of antiferromagnetic interactions p. The system exhibits ferromagnetic (F), a multitude of different chiral, spin-glass (S), and algebraically ordered (A) phases. The ferromagnetic and different chiral phases accumulate as different devil's staircases [10, 11] at their boundary with the disordered (D) phase. Note shallow and deep reentrances of disorder [66–70] at $p = 0.4$ and $p = 0.7$, respectively, surrounded by regular and temperature-inverted devil's staircases.

The full richness of the continuum of widely varying devil's staircase phase diagrams can best be seen in video form, four of which are accessible at http:// web.mit.edu/physics/berker/temperature_Delta_c0_scanp.avi, web.mit.edu/physics/berker/temperature_Delta_c05_scanp.avi, web.mit.edu/physics/berker/temperature_c_p1_scanDelta.avi, web.mit.edu/physics/berker/temperature_c_p0_scanDelta.avi These videos effectively exhibit a very large number of calculated phase diagram cross-sections.

V. ENTIRE-PHASE CRITICALITY, DIFFERENTIATED CHAOS IN THE SPIN-GLASS AND AT ITS BOUNDARY

The renormalization-group mechanism for the algebraically ordered (critical) phase is that, all renormalization-group trajectories originating inside this phase flow to a completely stable fixed point (sink) that occurs at finite temperature (finite coupling strength).[8, 9, 71–78] In all other ordered phases, the

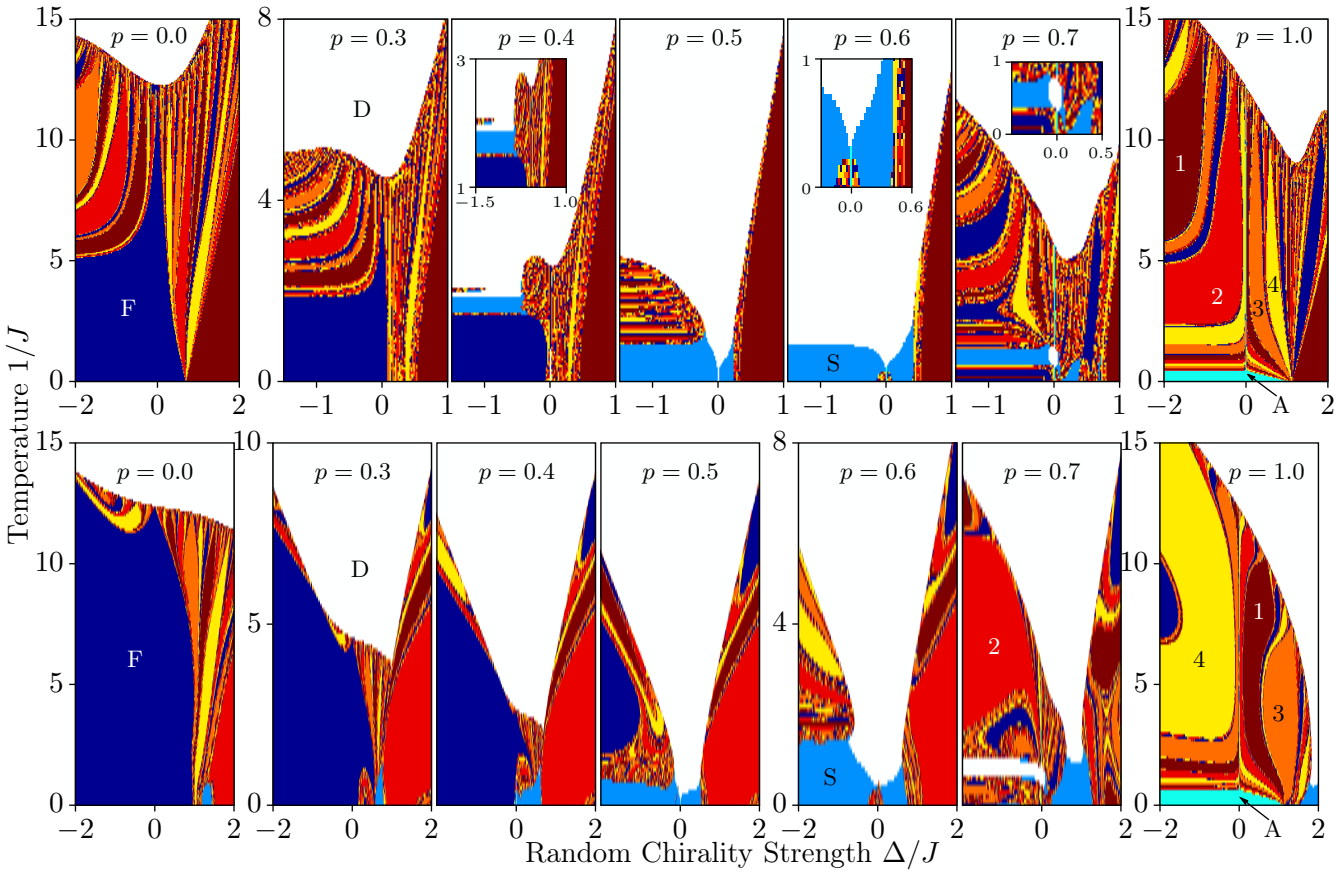

FIG. 3. (Color online) Calculated sequence of phase diagrams for the left-chiral ($c = 0$), on the upper side of the figure, and quenched random left- and right-chiral ($c = 0.5$), on the lower side, systems with quenched random ferromagnetic and antiferromagnetic interactions. The horizontal axis is the random chirality strength Δ/J. The consecutive phase diagrams are for different concentrations of antiferromagnetic interactions p. The system exhibits ferromagnetic (F), a multitude of different chiral, and spin-glass (S), and critical (algebraically) ordered (A) phases. On some of the chiral phases, the δ multiplicity of the asymptotically dominant interaction is indicated. The ferromagnetic and chiral phases accumulate as different devil's staircases at their boundary with the disordered (D) phase. Note shallow and deep reentrances of the disordered phase at $p = 0.4$ and $p = 0.7$, respectively, surrounded by regular and temperature-inverted devil's staircases. The full richness of the continuum of widely varying devil's staircase phase diagrams can also be seen in video form, four of which are accessible at http://web.mit.edu/physics/berker/temperature_Delta_c0_scanp.avi, web.mit.edu/physics/berker/temperature_Delta_c05_scanp.avi, web.mit.edu/physics/berker/temperature_c_p1_scanDelta.avi, web.mit.edu/physics/berker/temperature_c_p0_scanDelta.avi

trajectories flow to strong (infinite) coupling. In the ferromagnetic phase, the interaction $V_{ij}(0)$ becomes asymptotically dominant.

In the chiral phases, in the renormalization-group trajectories, one of the chiral interactions from the right-hand side of Eq. (4), $\{V_{ij}(\delta), V_{ij}(2\delta), V_{ij}(3\delta), V_{ij}(4\delta)\}$, becomes asymptotically dominant. However, in each of the separate phases, it takes a characteristic number n of renormalization-group transformations, namely a length scale of 3^n, to reach the dominance of one chiral interaction. Therefore, these chiral phases are distinct. After the dominance of one chiral interaction, the renormalization-group trajectory follows the periodic sequence $V_{ij}(\delta) \to V_{ij}(3\delta) \to V_{ij}(4\delta) \to V_{ij}(2\delta) \to V_{ij}(\delta)$ resulting from matching $q = 5$ and $b = 3$.

By contrast, the asymptotic flow in the spin-glass phase is to a strong-coupling fixed distribution $P(\mathbf{V}_{ij})$. Since, at each locality, the largest interaction in $\{V_{ij}(0), V_{ij}(\delta), V_{ij}(2\delta), V_{ij}(3\delta), V_{ij}(4\delta)\}$ is set to zero and the four other interactions are thus made negative, by subtracting the same constant from all five interactions without affecting the physics, the quenched probability distribution $P(\mathbf{V}_{ij})$, a function of five variables, is actually composed of five functions $P_\sigma(\mathbf{V}_{ij})$ of four variables, each such function corresponding to one of the interactions being zero and the other four, arguments of the function, being negative. Fig. 4 shows one of the latter functions: The part of the fixed distribution, $P_3(\mathbf{V}_{ij})$, for the interactions $\mathbf{V}_{ij}$ in which $V_{ij}(3\delta)$ is maximum and therefore 0 (and the other four interactions are negative) is shown in this figure. The projections of $P_3(\mathbf{V}_{ij})$ onto two of its four arguments are shown in each panel of

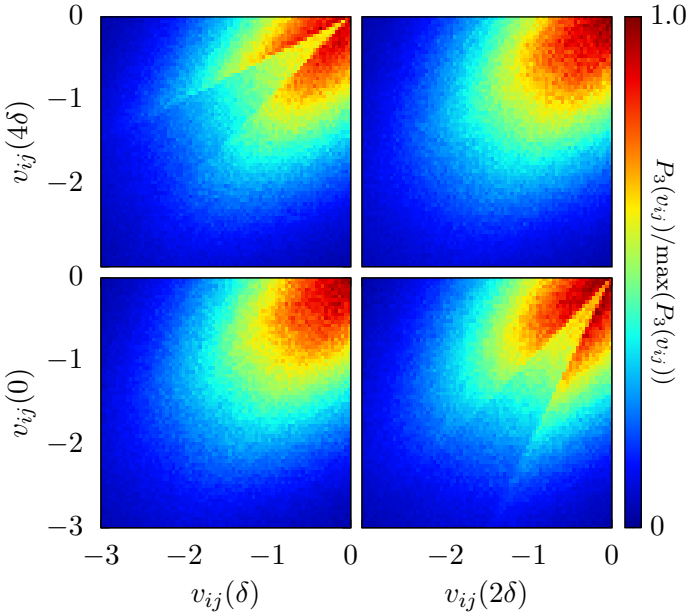

FIG. 4. (Color online) Asymptotic fixed distribution of the spin-glass phase. The part of the fixed distribution, $P_3(\mathbf{V}_{ij})$ for the interactions $\mathbf{V}_{ij}$ in which $V_{ij}(3\delta)$ is maximum and therefore 0 (and the other four interactions are negative) is shown in this figure, with $v_{ij}(\sigma\delta) = V_{ij}(\sigma\delta)/ < |V_{ij}(\sigma\delta)| >$. The projections of $P_3(\mathbf{V}_{ij})$ onto two of its four arguments are shown in each panel of this figure. The other four $P_\sigma(\mathbf{V}_{ij})$ have the same fixed distribution. Thus, chirality is broken locally, but not globally.

this figure. The other four $P_\sigma(\mathbf{V}_{ij})$ have the same fixed distribution. Thus, chirality is broken locally, but not globally.

Another distinctive mechanism, that of chaos under scale change [79–81] or, equivalently, under spatial translation [12], occurs within the spin-glass phase and differently at the spin-glass phase boundary [12], in systems with competing ferromagnetic and antiferromagnetic interactions [12, 64, 79–108] and, more recently, with competing left- and right-chiral interactions [6]. Fig. 5 gives the asymptotic chaotic renormalization-group trajectories of the spin-glass phase and of the phase boundary between the spin-glass and disordered phases. The five interactions $V_{ij}(0), V_{ij}(\delta), V_{ij}(2\delta), V_{ij}(3\delta), V_{ij}(4\delta)$ at a given location $< ij >$, under consecutive renormalization-group transformations, are shown. Chaos is measured by the Lyapunov exponent [12, 64, 99, 109, 110], which we here generalize, by the matrix form, to our multi-interaction case:

$$\lambda = \lim_{n\to\infty} \frac{1}{n} \ln \Big| \mathcal{E}\Big(\prod_{k=0}^{n-1} \frac{d\mathbf{v}_{k+1}}{d\mathbf{v}_k} \Big) \Big|, \qquad (8)$$

where the function $\mathcal{E}(\mathbf{M})$ gives the largest eigenvalue of its matrix argument $\mathbf{M}$ and the vector $\mathbf{v}_k$ is

$$\mathbf{v}_k = \{v_{ij}(0), v_{ij}(\delta), v_{ij}(2\delta), v_{ij}(3\delta), v_{ij}(4\delta)\}, \qquad (9)$$

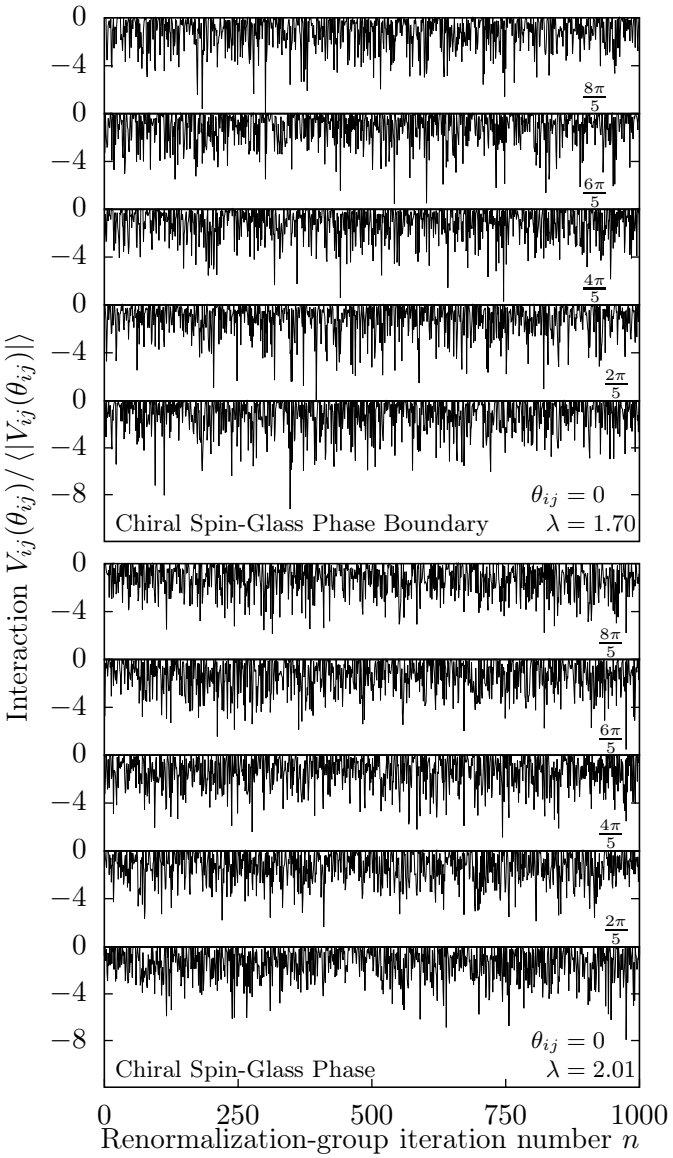

FIG. 5. Chaotic renormalization-group trajectories of the spin-glass phase (bottom) and of the phase boundary between the spin-glass and disordered phases (top). The five interactions $V_{ij}(0), V_{ij}(\delta), V_{ij}(2\delta), V_{ij}(3\delta), V_{ij}(4\delta)$ at a given location $< ij >$, under consecutive renormalization-group transformations, are shown. The $\theta_{ij} = \sigma\delta$ angular value of each interaction $V_{ij}(\theta_{ij})$ is indicated in the figure panels. Bottom panel: Inside the spin-glass phase. The corresponding Lyapunov exponent is $\lambda = 2.01$ and the average interaction diverges as $< V > \sim b^{y_R n}$, where n is the number of renormalization-group iterations and $y_R = 0.26$ is the runaway exponent. Top panel: At the phase boundary between the spin-glass and disordered phases. The corresponding Lyapunov exponent is $\lambda = 1.70$ and the average non-zero interaction remains fixed at $< V >= -0.99$. As indicated by the Lyapunov exponents, chaos is stronger inside the spin-glass phase than at its phase boundary.

with $v_{ij}(\sigma\delta) = V_{ij}(\sigma\delta)/ < |V_{ij}(\sigma\delta)| >$, at step k of the

renormalization-group trajectory. The product in Eq. (8) is to be taken within the asymptotic chaotic band, which is renormalization-group stable or unstable for the spin-glass phase or its boundary, respectively. Thus, we throw out the first 100 renormalization-group iterations to eliminate the transient points outside of, but leading to the chaotic band. Subsequently, typically using 1,000 renormalization-group iterations in the product in Eq. (8) assures the convergence of the Lyapunov exponent value λ. Spin-glass chaos occurs for $\lambda > 0$ [99] and the more positive λ, the stronger is chaos, as seen for example in the progressions in Figs. 6 and 7 of Ref. [64]. In the spin-glass phase of the currently studied system, the Lyapunov exponent is $\lambda = 2.01$ and the average interaction diverges as $< V > \sim b^{y_R n}$, where n is the number of renormalization-group iterations and $y_R = 0.26$ is the runaway exponent. At the phase boundary between the spin-glass and disordered phases, the Lyapunov exponent is $\lambda = 1.70$ and the average non-zero interaction remains fixed at $< V >= -0.99$. As indicated by the Lyapunov exponents, chaos is stronger inside the spin-glass phase than at its phase boundary.

VI. CONCLUSION

It is thus seen that chirality and chiral quenched randomness provides, in a simple model, remarkably rich phase transition phenomena. These include a multitude of chiral phases, continuum of widely varying devil's staircases, shallow and deep reentrances of the disordered phase surrounded by regular and temperature-inverted devil's staircases, a critical phase, and a chiral spin-glass phase with chaotic rescaling behavior inside and differently at its boundary. The widely varying continuum of devil's staircase phase diagrams are best seen in video form, four of which are accessible at http://web.mit.edu/physics/berker/temperature_Delta_c0_scanp.avi, web.mit.edu/physics/berker/temperature_Delta_c05_scanp.avi, web.mit.edu/physics/berker/temperature_c_p1_scanDelta.avi, web.mit.edu/physics/berker/temperature_c_p0_scanDelta.avi

ACKNOWLEDGMENTS

Support by the Academy of Sciences of Turkey (TÜBA) is gratefully acknowledged.

[1] S. Ostlund, Phys. Rev. **24**, 398 (1981).
[2] M. Kardar and A. N. Berker, Phys. Rev. Lett. **48**, 1552 (1982).
[3] D. A. Huse and M. E. Fisher, Phys. Rev. Lett. **49**, 793 (1982).
[4] D. A. Huse and M. E. Fisher, Phys. Rev. **29**, 239 (1984).
[5] R. G. Caflisch, A. N. Berker, and M. Kardar, Phys. Rev. B **31**, 4527 (1985).
[6] T. Çağlar and A. N. Berker, Phys. Rev. E **94**, 032121 (2016).
[7] H. Nishimori, *Statistical Physics of Spin Glasses and Information Processing* (Oxford University Press, Oxford, 2001).
[8] A. N. Berker and L. P. Kadanoff, J. Phys. A **13**, L259 (1980).
[9] A. N. Berker and L. P. Kadanoff, J. Phys. A **13**, 3786 (1980).
[10] P. Bak and R. Bruinsma, Phys. Rev. Lett. **49**, 249 (1982).
[11] A. Fukuda, Y. Takanishi, T. Isozaki, K. Ishikawa, and H. Takezoe, J. Mat. Chem. **4**, 997 (1994).
[12] E. Ilker and A. N. Berker, Phys. Rev. E **87**, 032124 (2013).
[13] E. Ilker and A. N. Berker, Phys. Rev. E **90**, 062112 (2014).
[14] C. Lupo and F. Ricci-Tersenghi, arXiv:1610.02014 [cond-mat.dis-nn] (2016).
[15] A. A. Migdal, Zh. Eksp. Teor. Fiz. **69**, 1457 (1975) [Sov. Phys. JETP **42**, 743 (1976)].
[16] L. P. Kadanoff, Ann. Phys. (N.Y.) **100**, 359 (1976).
[17] A. N. Berker and S. Ostlund, J. Phys. C **12**, 4961 (1979).
[18] R. B. Griffiths and M. Kaufman, Phys. Rev. B **26**, 5022R (1982).
[19] M. Kaufman and R. B. Griffiths, Phys. Rev. B **30**, 244 (1984).
[20] S. R. McKay and A. N. Berker, Phys. Rev. B **29**, 1315 (1984).
[21] M. Hinczewski and A. N. Berker, Phys. Rev. E **73**, 066126 (2006).
[22] M. Kaufman and H. T. Diep, Phys. Rev. E **84**, 051106 (2011).
[23] M. Kotorowicz and Y. Kozitsky, Cond. Matter Phys. **14**, 13801 (2011).
[24] J. Barre, J. Stat. Phys. **146**, 359 (2012).
[25] C. Monthus and T. Garel, J. Stat. Mech. - Theory and Experiment, P05002 (2012).
[26] Z. Z. Zhang, Y. B. Sheng, Z. Y. Hu, and G. R. Chen, Chaos **22**, 043129 (2012).
[27] S.-C. Chang and R. Shrock, Phys. Lett. A **377**, 671 (2013).
[28] Y.-L. Xu, L.-S. Wang, and X.-M. Kong, Phys. Rev. A **87**, 012312 (2013).
[29] S. Hwang, D.-S. Lee, and B. Kahng, Phys. Rev. E **87**, 022816 (2013).
[30] R. F. S. Andrade and H. J. Herrmann, Phys. Rev. E **87**, 042113 (2013).
[31] R. F. S. Andrade and H. J. Herrmann, Phys. Rev. E **88**, 042122 (2013).

[32] C. Monthus and T. Garel, J. Stat. Phys. - Theory and Experiment, P06007 (2013).
[33] O. Melchert and A. K. Hartmann, Eur. Phys. J. B **86**, 323 (2013).
[34] J.-Y. Fortin, J. Phys.-Condensed Matter **25**, 296004 (2013).
[35] Y. H. Wu, X. Li, Z. Z. Zhang, and Z. H. Rong, Chaos Solitons Fractals **56**, 91 (2013).
[36] P. N. Timonin, Low Temp. Phys. **40**, 36 (2014).
[37] B. Derrida and G. Giacomin, J. Stat. Phys. **154**, 286 (2014).
[38] M. F. Thorpe and R. B. Stinchcombe, Philos. Trans. Royal Soc. A - Math. Phys. Eng. Sciences **372**, 20120038 (2014).
[39] A. Efrat and M. Schwartz, Physica **414**, 137 (2014).
[40] C. Monthus and T. Garel, Phys. Rev. B **89**, 184408 (2014).
[41] T. Nogawa and T. Hasegawa, Phys. Rev. E **89**, 042803 (2014).
[42] M. L. Lyra, F. A. B. F. de Moura, I. N. de Oliveira, and M. Serva, Phys. Rev. E **89**, 052133 (2014).
[43] V. Singh and S. Boettcher, Phys. Rev. E **90**, 012117 (2014).
[44] Y.-L. Xu, X. Zhang, Z.-Q. Liu, K. Xiang-Mu, and R. Ting-Qi, Eur. Phys. J. B **87**, 132 (2014).
[45] Y. Hirose, A. Oguchi, and Y. Fukumoto, J. Phys. Soc. Japan **83**, 074716 (2014).
[46] V. S. T. Silva, R. F. S. Andrade, and S. R. Salinas, Phys. Rev. E **90**, 052112 (2014).
[47] Y. Hotta, Phys. Rev. E **90**, 052821 (2014).
[48] S. Boettcher, S. Falkner, and R. Portugal, Phys. Rev. A **91** 052330 (2015).
[49] S. Boettcher and C. T. Brunson, Eur. Phys. Lett. **110**, 26005 (2015).
[50] Y. Hirose, A. Ogushi, and Y. Fukumoto, J. Phys. Soc. Japan **84**, 104705 (2015).
[51] S. Boettcher and L. Shanshan, J. Phys. A **48**, 415001 (2015).
[52] A. Nandy and A. Chakrabarti, Phys. Lett. **379**, 43 (2015).
[53] D. Andelman and A. N. Berker, Phys. Rev. B **29**, 2630 (1984).
[54] M. J. P. Gingras and E. S. Sørensen, Phys. Rev. B. **46**, 3441 (1992).
[55] G. Migliorini and A. N. Berker, Phys. Rev. B. **57**, 426 (1998).
[56] M. J. P. Gingras and E. S. Sørensen, Phys. Rev. B. **57**, 10264 (1998).
[57] M. Hinczewski and A.N. Berker, Phys. Rev. B **72**, 144402 (2005).
[58] C. N. Kaplan and A. N. Berker, Phys. Rev. Lett. **100**, 027204 (2008).
[59] C. Güven, A. N. Berker, M. Hinczewski, and H. Nishimori, Phys. Rev. E **77**, 061110 (2008).
[60] M. Ohzeki, H. Nishimori, and A. N. Berker, Phys. Rev. E **77**, 061116 (2008).
[61] V. O. Özçelik and A. N. Berker, Phys. Rev. E **78**, 031104 (2008).
[62] G. Gülpınar and A. N. Berker, Phys. Rev. E **79**, 021110 (2009).
[63] C.N. Kaplan, M. Hinczewski, and A.N. Berker, Phys. Rev. E **79**, 061120 (2009).
[64] E. Ilker and A. N. Berker, Phys. Rev. E **89**, 042139 (2014).
[65] M. Demirtaş, A. Tuncer, and A. N. Berker, Phys. Rev. E **92**, 022136 (2015).
[66] P. E. Cladis, Phys. Rev. Lett. **35**, 48 (1975).
[67] F. Hardouin, A. M. Levelut, M. F. Achard, and G. Sigaud, J. Chim. Phys. **80**, 53 (1983).
[68] J. O. Indekeu, A. N. Berker, C. Chiang, and C. W. Garland, Phys. Rev. A **35**, 1371 (1987).
[69] R. R. Netz and A. N. Berker, Phys. Rev. Lett. **68**, 333 (1992).
[70] S. Kumari and S. Singh, Phase Transitions **88**, 1225 (2015).
[71] H. Saleur, Nucl. Phys. B **360**, 219 (1991).
[72] J. L. Jacobsen, J. Salas, and A. D. Sokal, J. Stat. Phys. **119**, 1153 (2005).
[73] J. L. Jacobsen and H. Saleur, Nucl. Phys. B **743**, 207 (2006).
[74] Y. Ikhlef, Mod. Phys. Lett. **25**, 291 (2011).
[75] J. L. Jacobsen and C. R. Scullard, J. Phys. A **45**, 494003 (2012).
[76] J. L. Jacobsen and J. Salas, Nucl. Phys. B **875**, 678 (2013).
[77] C. R. Scullard and J. L. Jacobsen, J. Phys. A **49**, 125003 (2016).
[78] R. Bondesan, S. Caracciolo, and A. Sportiello, arXiv:1608.02916 [cond-mat.stat-mech] (2016)
[79] S. R. McKay, A. N. Berker, and S. Kirkpatrick, Phys. Rev. Lett. **48**, 767 (1982).
[80] S. R. McKay, A. N. Berker, and S. Kirkpatrick, J. Appl. Phys. **53**, 7974 (1982).
[81] A. N. Berker and S. R. McKay, J. Stat. Phys. **36**, 787 (1984).
[82] A. J. Bray and M. A. Moore, Phys. Rev. Lett. **58**, 57 (1987).
[83] E. J. Hartford and S. R. McKay, J. Appl. Phys. 70, 6068 (1991).
[84] M. Nifle and H. J. Hilhorst, Phys. Rev. Lett. **68**, 2992 (1992).
[85] M. Nifle and H. J. Hilhorst, Physica A **194**, 462 (1993).
[86] M. Cieplak, M. S. Li, and J. R. Banavar, Phys. Rev. B **47**, 5022 (1993).
[87] F. Krzakala, Europhys. Lett. **66**, 847 (2004).
[88] F. Krzakala and J. P. Bouchaud, Europhys. Lett. **72**, 472 (2005).
[89] M. Sasaki, K. Hukushima, H. Yoshino, and H. Takayama, Phys. Rev. Lett. **95**, 267203 (2005).
[90] J. Lukic, E. Marinari, O. C. Martin, and S. Sabatini, J. Stat. Mech.: Theory Exp. L10001 (2006).
[91] P. Le Doussal, Phys. Rev. Lett. **96**, 235702 (2006).
[92] T. Rizzo and H. Yoshino, Phys. Rev. B **73**, 064416 (2006).
[93] H. G. Katzgraber and F. Krzakala, Phys. Rev. Lett. **98**, 017201 (2007).
[94] H. Yoshino and T. Rizzo, Phys. Rev. B **77**, 104429 (2008).
[95] J. H. Pixley and A. P. Young, Phys Rev B **78**, 014419 (2008).
[96] T. Aspelmeier, Phys. Rev. Lett. **100**, 117205 (2008).
[97] T. Aspelmeier, J. Phys. A **41**, 205005 (2008).
[98] T. Mora and L. Zdeborova, J. Stat. Phys. **131**, 1121 (2008).
[99] N. Aral and A. N. Berker, Phys. Rev. B **79**, 014434 (2009).

[100] Q. H. Chen, Phys. Rev. B **80**, 144420 (2009).
[101] T. Jörg and F. Krzakala, J. Stat. Mech.: Theory Exp. L01001 (2012).
[102] W. de Lima, G. Camelo-Neto, and S. Coutinho, Phys. Lett. A **377**, 2851 (2013).
[103] W. Wang, J. Machta, and H. G. Katzgraber, Phys. Rev. B **92**, 094410 (2015).
[104] V. Martin-Mayor and I. Hen, Scientific Repts. **5**, 15324 (2015).
[105] Z. Zhu, A. J. Ochoa, S. Schnabel, F. Hamze, and H. G. Katzgraber, Phys. Rev. A **93**, 012317 (2016).
[106] W. Wang, J. Machta, and H. G. Katzgraber, Phys. Rev. B **93**, 224414 (2016).
[107] J. Marshall, V. Martin-Mayor, and I. Hen, Phys. Rev. A **94**, 012320 (2016).
[108] L. A. Fernandez, E. Marinari, V. Martin-Mayor, G. Parisi, and D. Yllanes, arXiv:1605.03025 [cond-mat.dis-nn] (2016).
[109] P. Collet and J.-P. Eckmann, *Iterated Maps on the Interval as Dynamical Systems* (Birkhäuser, Boston, 1980).
[110] R. C. Hilborn, *Chaos and Nonlinear Dynamics*, 2nd ed. (Oxford University Press, New York, 2003).